Available online at www.sciencedirect.com
ScienceDirect
Applied Catalysis B: Environmental 78 (2008) 112–119
APPLIED CATALYSIS B: ENVIRONMENTAL
www.elsevier.com/locate/apcatb

The effect of N-doping and halide-doping on the activity of $CuCoO_4$ for the oxidation of elemental mercury

Zhijian Mei [a], Zhemin Shen [a,*], Zhiyuan Mei [b], Yejian Zhang [a], Fei Xiang [a], Jinping Chen [a], Wenhua Wang [a]

[a] School of Environmental Science and Engineering, Shanghai Jiao Tong University, 800 Dongchuan Road, Shanghai 200240, PR China
[b] Naval University of Engineering, Jiefang Road 717#, WuHan, Hubei 430033, PR China

Received 7 November 2006; received in revised form 5 September 2007; accepted 9 September 2007
Available online 14 September 2007

Abstract

The investigations for vapor-phase Hg^0 oxidation ability of Al_2O_3 (AL) loaded with $CuCoO_4$ (AL-C), $CuCoO_4 + NH_4Cl$ (AL-CCl), and $CuCoO_4 + NH_4Br$ (AL-CBr) are carried out in an attempt to produce more economical and effective sorbents for the control of Hg^0 emission from combustion processes. According to the X-ray diffraction (XRD), X-ray photoelectron spectroscopy (XPS), Brunauer–Emmett–Teller (BET) and mass balance analysis on mercury, we find that N-doped AL-C has bigger S_{BET} than AL-C and the nitrogen doping greatly improves AL-C's Hg^0 oxidation ability, especially at low temperatures. It is considered that nitrogen atoms in doped AL-C's polycrystalline are responsible for the significant enhancement in Hg^0 oxidation ability of AL-CCl and AL-CBr. The Hg^0 oxidation abilities of AL-CCl and AL-CBr under various adulteration values and adsorption temperatures were studied. When adulteration value is equal to 30%, AL-CCl and AL-CBr perform the best and their Hg^0 oxidation abilities are remarkably higher than AL-C over wide range temperatures. AL-CCl and AL-CBr's breakthrough times increases from AL-C's 26 h to 158 h and 208 h, respectively. The effects of 0.31% SO_2 on AL-C, AL-CCl and AL-CBr's Hg^0 oxidation abilities are insignificant, which indicates that N-doping has no adverse effect on both Co^{3+} and Cu^{2+}-octahedral cations structure.

Keywords: Mercury; N-dope; Gas-phase; $CuCoO_4$

1. Introduction

Recently, air emission of mercury has become the major source of adverse health effects of mercury, especially in coal combustors and municipal waste incinerators [1–3]. Environmental Protection Agency (EPA), as well as other regulatory agencies and health researchers, suggested a ''plausible link'' between anthropogenic sources emitting mercury and mercury methylation, bioaccumulation in the food chain, and adverse health effects on human beings and the wildlife [4,5]. Based on available evidence on health effects, EPA decided to regulate mercury released into the environment.

Many technologies have been applied to control the mercury emission of coal-fired power plants, such as air pollution control devices (APCDs) [6,7], sorbent injection (SI) [8–10], electro-catalytic oxidation (ECO) [11], photochemistry oxidation [12], oxidant injection, and catalytic oxidation [13,14], etc. Generally, oxidized mercury species are easier to be captured than Hg^0 due to their volatility, adsorption, adhesion, and so on. Therefore, increasing the gas-phase oxidized mercury proportion is very important for the improvement of efficiency in mercury control technologies. For example, increasing gas-phase oxidized mercury proportion will enhance overall mercury capture quantities in plants equipped with wet flue gas desulfuration (WFGD) systems. Development of novel catalyst can be used as an alternative to commercially available sorbents and oxidizing agents in order to enhance performance and reduce operation costs for sorbent injection mercury control systems used at coal-fired power plants. Many materials have been used to oxidize Hg^0, such as Pd, SCR, CuO, Cu_2O, V_2O_5, Cr_2O_3, MnO_2, MoO_3, Fe_2O_3, TiO_2, etc. [11,13–15]. Although Pd performs very well on oxidizing Hg^0 under full-scale applications, it is very expensive. Base metal oxides such

* Corresponding author. Tel.: +86 2127977572; fax: +86 2154742863.
E-mail addresses: meizhijian007@hotmail.com (Z. Mei), zmshen@sjtu.edu.cn (Z. Shen).

0926-3373/$ – see front matter © 2007 Elsevier B.V. All rights reserved.
doi:10.1016/j.apcatb.2007.09.003

as MnO_2, Fe_2O_3 perform unsatisfactorily when SO_2 exist. One of the unresolved problems in replacing noble metals with base metal oxides to full-scale applications is how to improve their SO_2 anti-poisoning ability and Hg^0 oxidation efficiency simultaneously.

Recently, nonmetal-doping technology has become a rapidly growing field of interest [16–18]. Asahi et al. [17] predicted by first-principle calculations and demonstrated in experiments that nitrogen-doped TiO_2 could lower its band gap and exhibited enhanced photoactivity under visible-light irradiation. Valentin et al. [19] compared the electronic structure of N-doped anatase and rutile TiO_2, and elucidated the origin of the experimental change observed in photo-activities of anatase and rutile TiO_2 induced by substitutional N-doping. Other nonmetal atoms, such as C [20], S [21], just as N atom, can be doped into metal oxide matrix as anions and substitute for O atoms.

Halide-doped catalysts, such as $La_{1.85}Sr_{0.15}CuO_{4-\delta}X_\sigma$ (X = F, Cl), $Nd_{1.85}Ce_{0.15}CuO_{4-\delta}X_\sigma$ (X = F, Cl), $La_{1-x}Sr_xFeO_{3-\delta}X_\sigma$ (X = F, Cl), $SrFeO_{3-\delta}Cl_\sigma$, and $YBa_2Cu_3O_{7-\delta}X_\sigma$(X = = F, Cl) have been used to oxidize selectively ethane to ethene [22,23]. Although the introduction of halide ions in limited amount does not induce any phase transformation or any significant change in surface area, there are changes in lattice parameters. Dai realized that the doping of halide ions had caused (i) the Cu^{3+} content in $La_{1.85}Sr_{0.15}CuO_{4-\delta}$ to rise, (ii) the Cu^+ content in $Nd_{1.85}Ce_{0.15}CuO_{4-\delta}$ to fall, and (iii) the oxygen vacancy density to decrease.

Our previous work manifested that mixed oxides $Cu_xCo_{3-x}O_4$ ($0 < x < 1$) had low activity for oxidizing Hg^0, especially at low temperatures (data not published yet), which was not cost-efficiency and would constrict their application, although they had outstanding SO_2 anti-poisoning ability [24,25]. The aim of this study is to use N-doping technology to improve $CuCoO_4$'s Hg^0 oxidation ability, especially at low temperatures (<523 K). The effects of NH_4Cl or NH_4Br adulteration values, adsorption temperatures and SO_2 on N-doped $CuCoO_4$'s Hg^0 oxidation ability are carefully studied. Based on the experiment results, possible Hg^0 oxidation mechanism of N-doped $CuCoO_4$ is provided.

2. Experimental

2.1. Sample preparation

The commercially available $Al(OH)_3$ which was purchased from Shanghai Reagent Corporation of China was decomposed at 1073 K for 24 h. The produce γ-Al_2O_3 was stored in a desiccator prior to adsorption experiments.

$CuCoO_4$ loaded on γ-Al_2O_3 (AL-C) was prepared by the thermal decomposition of Cu–nitrate/Co–nitrate mixtures loaded on γ-Al_2O_3. Both nitrates were mixed in Co/Cu atomic ratio of 1. The mixtures were dissolved in water to form the mixtures solution. γ-Al_2O_3 was impregnated by the mixtures solution in proportion to 20 wt% nitrate loading values and heated to 503 K, the temperature at which nitrogen oxides were evolved. The heterogeneous mass obtained was ground in a mortar and heated for 5 h at 673 K.

$CuCoO_4 + NH_4Cl$ loaded on γ-Al_2O_3 (AL-CCl) was prepared by impregnating AL-C with NH_4Cl solutions corresponding to different Cl/Cu atomic ratios before the decomposition and dried at 333 K, and then calcined at 673 K for 3 h. The preparation of $CuCoO_4 + NH_4Br$ loaded on γ-Al_2O_3 (AL-CBr) was similar to AL-CCl.

The blank sample NH_4Cl or NH_4Br loaded on γ-Al_2O_3 (AL-Cl or AL-Br) was prepared by impregnating γ-Al_2O_3 with 4 wt% NH_4Cl or NH_4Br, respectively. Impregnated γ-Al_2O_3 was dried in an oven at 333.2 K and then calcined at 673.2 K for 3 h. After being cooled down to the room temperature, AL-Cl or AL-Br was stored in a desiccator before usage. All chemicals used above were in analytical grade.

2.2. Analytical method

The crystal structures of the sorbents were determined by an X-ray diffractometer (XRD, AXS DS Discover, Bruker) operating at 40 kV and 40 mA using Cu Kα radiation. The patterns recorded were referred to the powder diffraction files PDF-2 database for the identification of crystal phases. X-ray photoelectron spectroscopy (XPS, VG Scientific Microlab 310F system) was used to determine the N 1s, Co 2p, Cu 2p, and Hg 4f7 binding energies of surface nitrogen, cobalt, copper, and mercury species, respectively, with Mg Kα ($h\nu$ = 1253.6 eV) as the excitation source. The instrumental resolution was 1 eV. The C 1s line at 284.6 eV was taken as a reference for binding energy calibration. The Brunauer–Emmett–Teller (BET) specific surface area (S_{BET}) and pore size distribution were determined using nitrogen adsorption apparatus (Micromeritics ASAP 2010). All the samples were degassed at 453 K prior to BET measurements. The size and shape of the particles were observed using scanning electron microscopy (SEM, LEO 1550 VP). The vapor-phase Hg^0 concentrations were analyzed continuously using a cold vapor atomic absorption spectrophotometry analyzer (CVAAS, SG-921). The total mercury concentration of spent samples was determined using advanced mercury analyzer (AMA254, America). AMA254 is a single purpose atomic absorption spectrophotometer for mercury determination. It is designated for the direct mercury determination in solid and liquid samples without a need of sample chemical pre-treatment (mineralization, etc.).

2.3. Catalytic test

The assembly for catalytic tests consists of an elemental mercury permeation tube, a packed-bed reactor, an on-line CVAAS, and a data acquisition system. The reactor scheme is shown in Fig. 1. A flow of simulated flue gas passes the permeation tube and yields a stable concentration of mercury. The reactor (adsorber) is a quartz tube (76.2 cm. in length with an outer diameter of 0.508 cm. and inner diameter of 0.423 cm) held in a vertical position. Quartz has good chemical resistance and inertness toward elemental mercury [14]. The reactor is

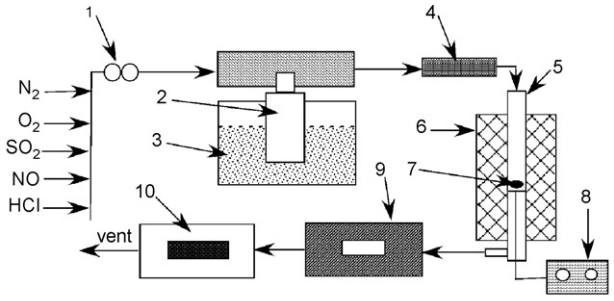

1. Mass Flow Control; 2. Hg^0 Permeation Tube; 3. Oil Heating Bath; 4. Heating Tape; 5. Tubular Reactor; 6. Furnace; 7. Catalyst; 8. Temperature Monitor; 9. CVAAS; 10. Activated Carbon Trap.

Fig. 1. Schematic of the experimental setup. CVAAS: SG-921 cold vapor atomic absorption spectrophotometry detects the gas-phase Hg^0 concentration on line. Simulated gas: the gas includes two kinds of composition. One is 5.0 vol.% oxygen and N_2 acts as balance gas. The other is 158 ppmv CO, 230 ppmv NO, 5.0 vol.% O_2, 0.31 vol.% SO_2 and the rest being N_2. Mass flow meter: control the quantity of gas flow. Hg permeation tube holder: control Hg^0 emission rate. Vertical packed bed of sorbent: the main reaction place where sorbents are placed and adsorption temperature is under control. Activated carbon trap: capture the mercury in the effluent to eliminate pollution.

surrounded by a large clam-shell furnace. A temperature control device is employed to keep the adsorbent bed at desired temperatures. Simulated gas passes the permeation tube holder and enters CVAAS to determine the baseline. Once thermal stability is reached, simulated gas is diverted to pass through the adsorbent bed for adsorption test.

Some kinetic parameters for Hg^0 oxidation were obtained under condition 1 with influent gas stream of 6 L h^{-1}. The composition of the inlet gas included 5.0% of oxygen, 0.126 ppm Hg^0, and the rest being N_2. The other catalytic tests processed under condition 2 with gas stream of 6 L h^{-1}. The composition of the inlet gas which is close to the flue gas of coal-fire plant included 158 ppmv CO, 230 ppmv NO, 0.035 ppm Hg^0, 5.0% O_2 and the rest being N_2. The catalyst mass was 0.02 g and the used fraction was between 0.5 mm and 0.6 mm. The adsorption temperatures varied from 373 K to 723 K. For SO_2 poisoning test, 0.31% sulphur dioxide, corresponding to the typical concentration in coal-fire plant flue gas, was introduced into the influent.

3. Results and discussion

3.1. Catalyst characterization

The data of pore size in Table 1 resulted mainly from a variety of accumulated pore voids between particles and particles with different dopants. These pores allow rapid diffusion of various gaseous reactants and products during Hg^0 oxidation reaction and enhance the Hg^0 oxidation rate. It can be seen from Table 1 that γ-Al_2O_3 powders show the biggest S_{BET} value of 72.3 m^2 g^{-1}. However, the surface area and pore volume became smaller with the loading of $CuCoO_4$ and the pore diameter increases due to the growth of $CuCoO_4$ crystallites. When AL-C doped with 30% NH_4Cl or NH_4Br, its S_{BET} and pore volume both increase.

The SEM photograph of AL-C powders prepared by the decomposition of mixtures of equal proportions of copper and cobalt nitrates loaded on γ-Al_2O_3 is shown in Fig. 2. When doped with 30% NH_4Cl or NH_4Br, the size of the particles on AL-C surface decreases from 20 μm to 4 μm, which causes their S_{BET} and pore volume to increase. Moreover, AC-CCl and AC-CBr become less electric than AC-C, which means that NH_4Cl and NH_4Br have changed the surface electric state of AL-C.

The X-ray diffractograms (XRD) data of AL-C and 30% NH_4Cl or NH_4Br doped AL-C were analyzed using crystallographica search-match and the results are shown in Table 2. It can be seen that, although there exist different $Cu_xCo_{3-x}O_4$ ($x < 1$) and CuO in AL-C, all the $Cu_xCo_{3-x}O_4$ ($x < 1$) show only the pattern of a cubic spinel. This indicates that the copper introduced is completely in the spinel phase. The doping of 30% NH_4Cl makes the phases of AL-C change greatly. At first, there was not CuO and $CuCo_2O_4$ cubic spinel. Later, the x value of $Cu_xCo_{3-x}O_4$ ($x < 1$) changed. At last, AL-CCl contained $CoCuO_4$ which was rhombohedral. For AL-CBr, there exists no possible phase matching the XRD spectrum. Obviously, NH_4Br has greater effect on the crystal structure of AL-C than NH_4Cl. The XRD results show that there have not been any detectable dopant-related peaks. The dopants may have moved into either the interstitial positions or the substitutional sites of the $CuCoO_4$ crystal structure.

XPS measurements of the N 1s binding energy indicate that there have been two sets of N peaks at 396–398 eV and 400–402 eV, respectively (Fig. 3). The former set of peaks at 396–398 eV is similar to Ti–N bonds in TiO_2 where the peak is at 397 eV. This set of peaks can be attributed to N–Co or N–Cu bond in N-doped AL-C. Since XRD does not indicate the presence of CoN or CuN phase, the oxygen sites must be occupied by nitrogen atoms on the surface. The latter set of peaks at 400–402 eV suggests the presence of chemisorbed N_2 molecules on the surface [26].

AL-C's Co 2p spectrum exhibits five peaks in the sites 780 eV, 782 eV, 784 eV, 796.4 eV, and 800 eV, respectively (Fig. 4). When doped with NH_4Cl or NH_4Br, the peaks at 782 eV and 784 eV disappear. This phenomenon is similar to

Table 1
Effect of NH_4Cl/NH_4Br on the BET surface and pore parameters of AL-C powders

Sample	Surface area (m^2 g^{-1})	Pore volume (mL g^{-1})	Pore size (nm)
γ-Al_2O_3	72.3	0.249	13.8
AL-C	53.3	0.189	14.2
AL-CCl	57	0.2	14
AL-CBr	58	0.198	14.3

Table 2
The XRD analysis results of AL-C and doped with 30% NH_4Cl and NH_4Br

Sample	The existent phases (strong → weak)
AL-C	$CuCo_2O_4$ (cube) → CuO (cube) → $Cu_{0.95}Co_{2.05}O_4$ (cube) → $Cu_{0.75}Co_{2.25}O_4$ (cube) → $Cu_{0.15}Co_{2.84}O_4$ (cube)
AL-CCl	$Cu_{0.37}Co_{2.63}O_4$ (cube) → $Cu_{0.76}Co_{2.24}O_4$ (cube) → $Cu_{0.72}Co_{2.28}O_4$ (cube) → $CoCuO_4$ (rhombohedral)
AL-CBr	Non

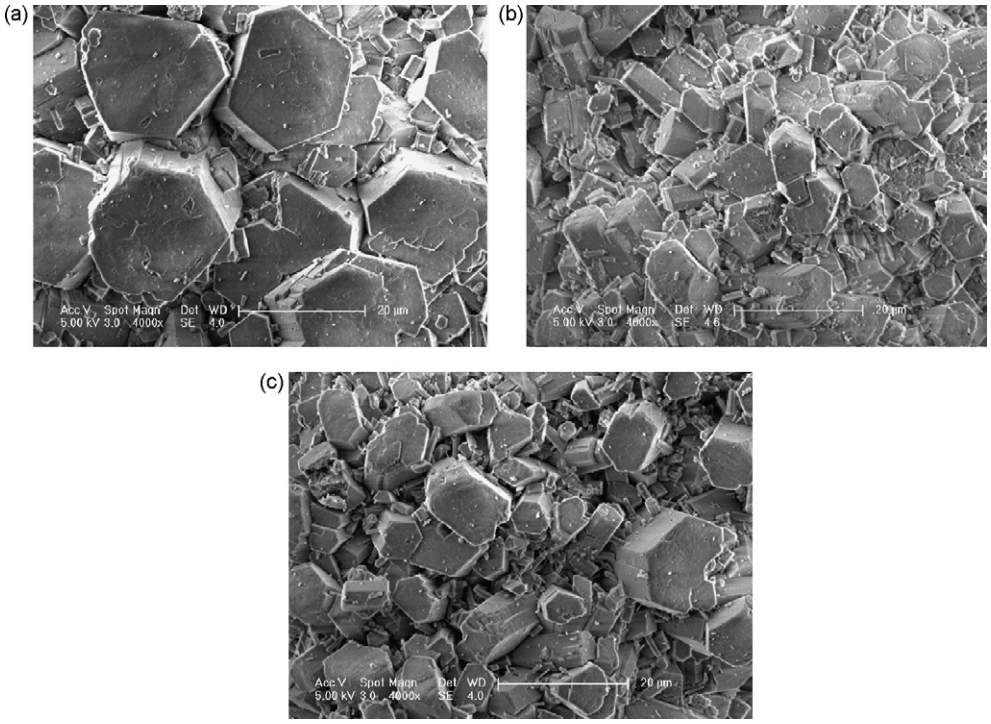

Fig. 2. The SEM analysis of (a) AL-C, (b) AL-CCl (χ = 30%), and (c) AL-CBr (χ = 30%). (a) The SEM analysis of $CuCoO_4$ loaded on γ-Al_2O_3 decomposed at 673 K for 3 h. (b) The SEM analysis of 30 mol% NH_4Cl doped $CuCoO_4$ loaded on γ-Al_2O_3 decomposed at 673 K for 3 h. (c) The SEM analysis of 30% NH_4Br doped $CuCoO_4$ loaded on γ-Al_2O_3 decomposed at 673 K for 3 h.

the relationship between Co_3O_4 (780 eV, 781.6 eV, 795.6 eV, and 797 eV) and $Co(NO_3)_2$ (780 eV, 797 eV). AL-CCl and AL-CBr's Co 2p XPS peak configurations are similar to $Co(NO)_3$ which is not detected through XRD. This XPS results indicate, from a different perspective, that the oxygen sites of AL-C are partly occupied by nitrogen atoms. Another observation is that AL-CCl and AL-CBr's Co 2p binding energy at 799.6 eV is lower than AL-C's Co 2p binding energy at 800 eV.

The Cu 2p binding energy data of different sorbents are shown in Fig. 5. For AL-C, the Cu 2p spectrum exhibits four peaks in the sites 932 eV, 942.8 eV, 948 eV, and 952 eV, respectively. However, AL-CCl or AL-CBr's Cu 2p binding energy is lower than the corresponding binding energy of AL-C. This phenomenon can be explained by charge transfer. Overall, the increase of charge density on Cu atoms causes the binding energy to decrease. Therefore, the NH_4Cl or NH_4Br

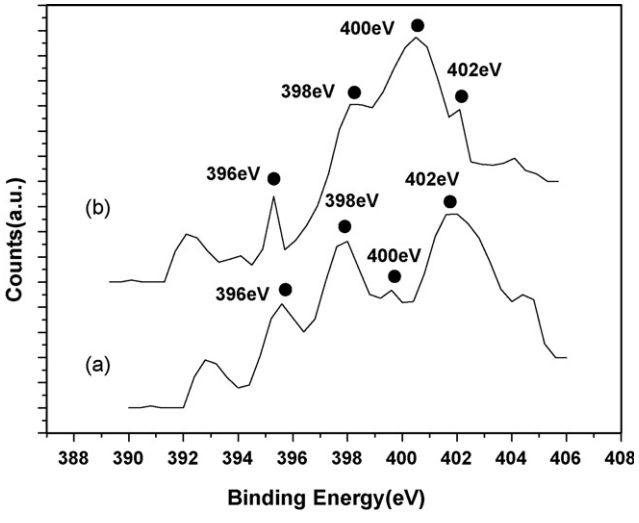

Fig. 3. N 1s XPS spectra of (a) AL-CBr (χ = 30%) and (b) AL-CCl (χ = 30%). (a) The N 1s XPS spectra of 30% NH_4Br doped $CuCoO_4$ loaded on γ-Al_2O_3 decomposed at 673 K for 3 h. (b) The N 1s XPS spectra of 30% NH_4Cl doped $CuCoO_4$ loaded on γ-Al_2O_3 decomposed at 673 K for 3 h.

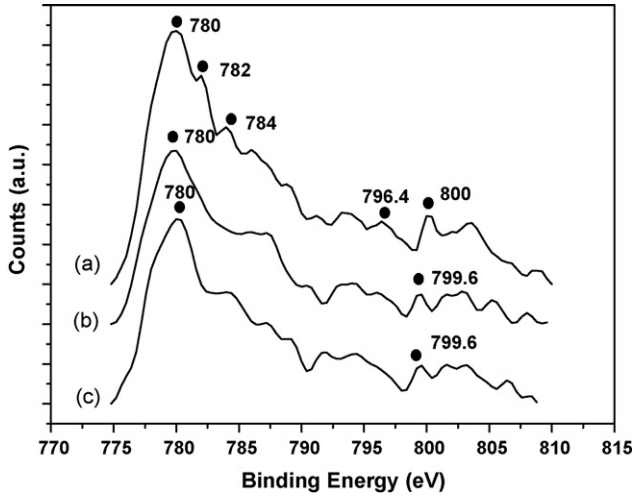

Fig. 4. Co 2p XPS spectra of (a) AL-C, (b) AL-CCl (χ = 30%), and (c) AL-CBr (χ = 30%). (a) The Co 2p XPS spectra of $CuCoO_4$ loaded on γ-Al_2O_3 decomposed at 673 K for 3 h. (b) The Co 2p XPS spectra of 30% NH_4Cl doped $CuCoO_4$ loaded on γ-Al_2O_3 decomposed at 673 K for 3 h. (c) The Co 2p XPS spectra of 30% NH_4Br doped $CuCoO_4$ loaded on γ-Al_2O_3 decomposed at 673 K for 3 h.

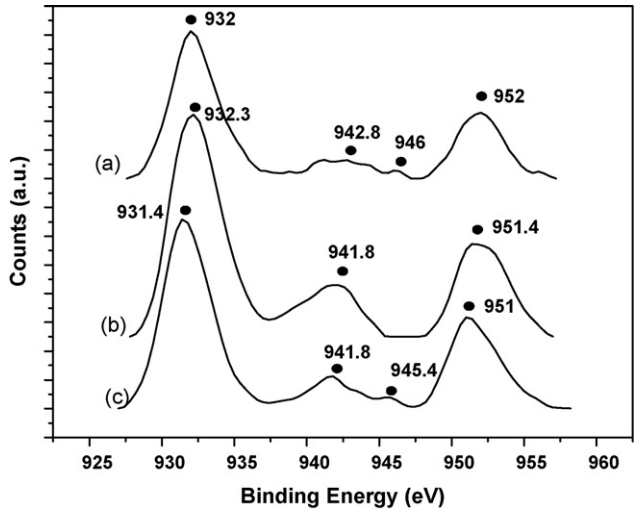

Fig. 5. Cu 2p XPS spectra of (a) AL-C, (b) AL-CCl (χ = 30%), and (c) AL-CBr (χ = 30%). (a) The Cu 2p XPS spectra of $CuCoO_4$ loaded on γ-Al_2O_3 decomposed at 673 K for 3 h. (b) The Cu 2p XPS spectra of 30% NH_4Cl doped $CuCoO_4$ loaded on γ-Al_2O_3 decomposed at 673 K for 3 h. (c) The Cu 2p XPS spectra of 30% NH_4Br doped $CuCoO_4$ loaded on γ-Al_2O_3 decomposed at 673 K for 3 h.

doping weakens the copper–oxygen bonds and lattice O^{2-} becomes more active. This will be discussed in detail later. Based on the above analysis, the N-doping processes can be expressed as follows where $CuCo_2O_4$ is considered to be the main active component:

$$Cu(NO_3)_2 + Co(NO_3)_2 + NH_4Cl \rightarrow CuCo_2N_xO_{4-x} + CuN_yO_{1-y} + N_{2ad} + Cl_{ad}^- + \text{other} \quad (1)$$

$$Cu(NO_3)_2 + Co(NO_3)_2 + NH_4Br \rightarrow CuCo_2N_xO_{4-x} + CuN_yO_{1-y} + N_{2ad} + Br_{ad}^- + \text{other} \quad (2)$$

Wherein $CuCo_2N_xO_{4-x}$ is the N-doped $CuCo_2O_4$, N_{2ad} is the chemisorbed N_2 molecules on the surface, Cl_{ad}^- or Br_{ad}^- is the chemisorbed anion Cl^- or Br^- on the surface.

3.2. Effect of NH_4Cl/NH_4Br concentration

The relationship between Hg^0 oxidation ability (η) and adulteration ratio (χ) of AL-CCl and AL-CBr were investigated. The performances of different AL-CCl and AL-CBr are shown in Fig. 6, where χ is defined as follows:

$$\chi(\%) = \frac{n_{NH_4Cl/NH_4Br}}{n_{Cu}} \times 100 \quad (3)$$

Wherein n_{NH_4Cl/NH_4Br} is the quantity of NH_4Cl or NH_4Br (mol) and n_{Cu} is the quantity of Cu^{2+} (mol).

η is defined as follows:

$$\eta(\%) = \frac{Hg_{inlet} - Hg_{outlet}}{Hg_{inlet}} \times 100 \quad (4)$$

Wherein Hg_{inlet} is the quantity of inlet Hg^0 (mol) and Hg_{outlet} is the quantity of outlet Hg^0 (mol).

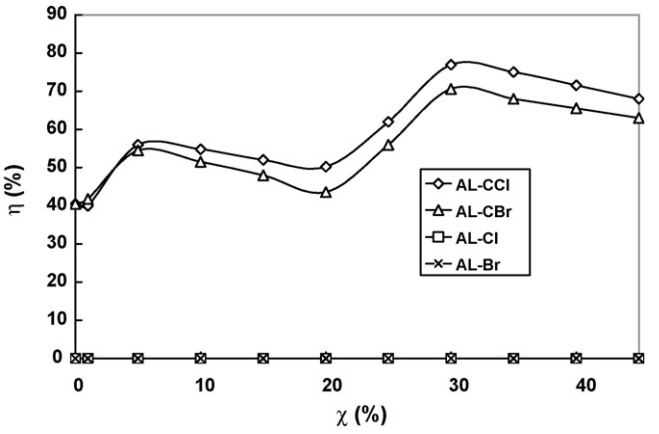

Fig. 6. Hg^0 oxidation ability (η) vs. adulteration ratio (χ) of AL-CCl and AL-CBr at 523 K. AL-CCl: the Hg^0 oxidation ability (η) of AL-CCl at different adulteration ratio (χ). AL-CBr: the Hg^0 oxidation ability (η) of AL-CBr at different adulteration ratio (χ).

NH_4Cl and NH_4Br have similar effect on AL-C's Hg^0 oxidation ability. Both of AL-CCl and AL-CBr's Hg^0 oxidation ability have two maximums where χ is equal to 5% and 30%, respectively. When χ reaches 30%, AL-CCl or AL-CBr shows the highest Hg^0 oxidation ability and reaches 76.9% or 70.6%, respectively, which are notably higher than AL-C's 40.5%. Continually increasing χ above 30% has adverse effect on their Hg^0 oxidation ability and will increase operation costs. Therefore, 30% is regarded as the optimal value which will be used as default value in later experiments. This phenomenon indicates that the control mechanism affecting Hg^0 oxidation ability of AL-CCl or AL-CBr is the same. Through XPS analysis, we consider N-doping to be the main mechanism responsible for AL-CCl and AL-CBr's activity increase. The small difference between AL-CCl and AL-CBr may have been caused by the anion Cl^- and Br^-, which will be discussed later.

Performances of AL-Cl or AL-Br indicate that anion Cl^- or Br^-'s Hg^0 oxidation ability is poor (Fig. 6), which is different from the situation of Br^- or Cl^- impregnated on activated carbon where they can largely improve activated carbon's elemental mercury capture ability [27,28]. Based on previous works [8,29], the mechanism of chemisorption of elemental mercury onto the anion-impregnated activated carbons is proposed as follows: Cl^- or Br^- is reduced by the carbon contents in activated carbons and some anion-contained complexes are formed which can react with Hg^0. Because γ-Al_2O_3 lacks such activation groups, AL-Cl or AL-Br cannot activate the anion to oxidize Hg^0. Therefore, AL-CCl and AL-CBr's Hg^0 oxidation ability increase does not originate from the pure anion directly reacting with Hg^0. The inproportional improvement of Hg^0 oxidation ability to the amount of NH_4Cl or NH_4Br also supports the above view point.

3.3. Temperature effect

Investigations in Hg^0 oxidation by AL-C, AL-CCl and AL-CBr were carried out to observe the changes of performances over a wide range of temperatures (373–723 K). The

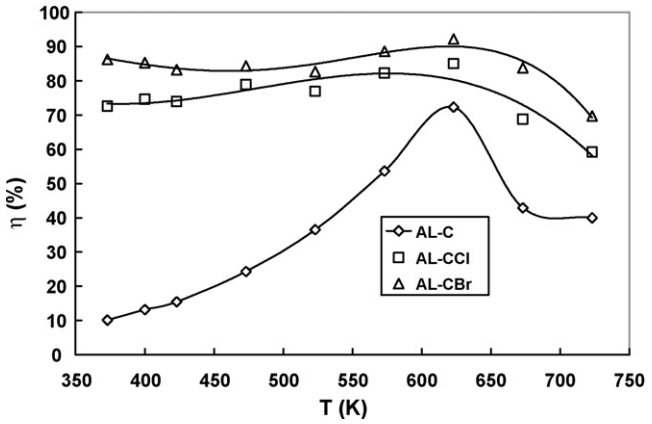

Fig. 7. Hg^0 oxidation ability (η) vs. adsorption temperature T of AL-C, AL-CCl (χ = 30%) and AL-CBr (χ = 30%). AL-C: the Hg^0 oxidation ability (η) of AL-C at different adsorption temperatures. AL-CCl: the Hg^0 oxidation ability (η) of 30% NH_4Cl doped AL-C at different adsorption temperatures. AL-CBr: the Hg^0 oxidation ability (η) of 30% NH_4Br doped AL-C at different adsorption temperatures.

experimental results are shown in Fig. 7. When adsorption temperature increased from 373 K to 623 K, AL-C's Hg^0 oxidation ability increased from 12.1% to 72.3%. However, the performances of AL-CCl and AL-CBr are different from that of AL-C and their Hg^0 oxidation abilities are independent of adsorption temperatures. Previous studies manifested that the reaction between chloride and elemental mercury showed an exothermic behavior [8,29]. Low temperatures are beneficial to the reaction between Hg^0 and NH_4Cl. AL-CCl or AL-CBr's Hg^0 oxidation ability at low adsorption temperatures may be attributed to the reaction between Hg^0 and Cl_{ad}^- or Br_{ad}^-. High temperatures are beneficial to the reaction between oxygen and Hg^0 which is catalyzed by $CuCo_2N_xO_{4-x}$. Above 623 K, the Hg^0 oxidation abilities of all sorbents decrease. The possible reason is that mercuric oxide is catalytically decomposed by $CuCo_2O_4$ or $CuCo_2N_xO_{4-x}$ and higher temperatures are beneficial to mercuric oxide decomposition [1].

Compared with AL-C, the Hg^0 oxidation ability of AL-CCl and AL-CBr is significantly higher, especially at low temperatures. The temperature independence of AL-CCl and AL-CBr indicates that N-doping greatly lowers the active energy of oxidation reaction. This property of AL-CCl and AL-CBr makes them ideal wide-range materials to control Hg^0 emission, especially at low temperatures.

3.4. Hg^0 adsorption analysis

Oxidized mercury has been found in the effluent using chloride-impregnated activated carbon as sorbent under downflow fix-bed conditions and the total concentration of oxidized mercury species (Hg_{ox}) in the effluent increased significantly with the increase in chloride content. Release of oxidized mercury species into the effluent can be the result of either a weak carbon–chloride bond or weak chloride–mercury bond or both [8]. Therefore, it is necessary to take into account of the actual Hg^0 captured by different sorbents and this is done

Table 3
Comparison of Hg capture ability (θ) with Hg oxidation ability (η) of different samples at 623 K and the influence of SO_2 on conversion efficiency over different samples under condition 2

Sample	η (%)	θ (%)	$\Phi 1$[a] (%)	$\Phi 2$[a] (%)	R_{SO_2}	Breakthrough time (h)
CuO	N/A	N/A	N/A	N/A	0	8
Co_3O_4	N/A	N/A	N/A	N/A	0	10
AL-C	72.3	69.2	10.1	3.1	0.94	26
AL-CCl	85	76.4	36.4	8.6	0.96	158
AL-CBr	92.2	84.2	50.6	8	1	208

[a] The ratio of oxidized mercury in the effluent divided effluent total mercury.

by calculating the Hg capture ability (θ) of the catalysts according to the following formula:

$$\theta(\%) = \frac{q}{Q} \times 100 \quad (5)$$

Wherein q is the total quantity of Hg captured by the catalysts (g) and Q is the total inlet quantity of Hg^0 (g) which is estimated by

$$Q = V \times C \times t \quad (6)$$

Wherein t is the reaction time, V the gas flow (L h^{-1}) and C is the inlet concentration of Hg^0 (%).

The results of Hg capture ability (θ) versus Hg oxidation ability (η) are shown in Table 3. The mass balance analyses on mercury enlighten that, for all sorbents, there does exist some oxidized mercury released into the gas again due to the high adsorption temperature.

The other observation is that AL-C has better oxidized mercury capture ability, because its $\Phi 1$ and $\Phi 2$ are both less than AL-CCl and AL-CBr. Compared with AL-C, the oxidized mercury percentage in the effluent of AL-CCl or AL-CBr increases from 10.1% to 36.4% or 50.6%, respectively. This may be caused by the following two reasons. First, the $CuCo_2N_xO_{4-x}$ has less affinity for oxidized mercury than $CuCo_2O_4$. Secondly, the anion Cl^- or Br^- takes part in the Hg^0 oxidation reaction which increases AL-CCl and AL-CBr's Hg^0 oxidation ability but decreases their oxidized mercury capture ability, because Vidic found that using copper chloride-impregnated activated carbon adsorbed Hg^0 at 423 K, the $\Phi 1$ ranged between 15% and 26% [8].

The breakthrough times (defined as Co/Ci = 95%) of different sorbents are listed in Table 3. Under the same adsorption condition, AL-CCl and AL-CBr's breakthrough times increase from AL-C's 26 h to 158 h and 208 h, respectively. The reasons may lie in the following two factors. First, N-doping greatly increases the active centre numbers of AL-C. It can be inferred from Table 1 that AL-CCl and AL-CBr have bigger S_{BET} than AL-C. Secondly, AL-CCl and AL-CBr's active centers have less affinity for the oxidation produce. Based on the above experiment results, AL-CCl and AL-CBr are more cost-efficient than AL-C if applied to pilot-scale or full-scale mercury treatment operation.

3.5. The effect of SO_2

In this part, the effects of dopants NH_4Cl and NH_4Br on AL-C's SO_2 anti-poisoning ability are discussed. It is found convenient to characterize the resistance using the following experimental test. From the curves presented in Fig. 7, the temperature, where the biggest conversion is attained, can be determined. For every sorbent, the corresponding temperature has been adjusted and after stabilizing the conversion ($n_{\text{initial}}^{\max}$), SO_2 is introduced in the inlet gas mixture for 120 min. At the end of this test period, the reduced conversion rate ($n_{\text{final}}^{\text{reduced}}$) is checked. Then, the ratio $R_{SO_2} = n_{\text{final}}^{\text{reduced}}/n_{\text{initial}}^{\max}$ serves as an index measuring the resistance of the catalysts towards SO_2 poisoning. Different sorbents' R_{SO_2} ranges from 0 to 1 under condition 2 (Table 3).

As can be seen, AL-C, AL-CCl and AL-CBr all possess excellent SO_2 anti-poisoning ability. In previous works, it was shown that when the x of $Cu_xCo_{3-x}O_4$ ($x < 1$) was above 0.2, the Cu^{2+} ions were distributed over both tetrahedral and octahedral cationic sites of the spinel lattice [30]. Therefore, the poison resistant active sites can be correlated to both Co^{3+} and Cu^{2+}-octahedral cations on the surface of the spinels [25]. The results of SO_2 poisoning tests show that dopants NH_4Cl and NH_4Br have not any adverse effect on the SO_2 anti-poisoning ability of $CuCoO_4$ which indicate that N-doping only replace crystal oxygen or oxygen vacancies and affect neither Co^{3+} nor Cu^{2+}-octahedral cations structure.

3.6. Reaction mechanism

The spent AL-C, AL-CCl and AL-CBr were analyzed through XPS to find out the adsorbed mercury species. The results are shown in Fig. 8. The spent AL-C's XPS measurements of the Hg 4f7 binding energy (peak at 100.8 eV) indicate that the adsorption mercury species is

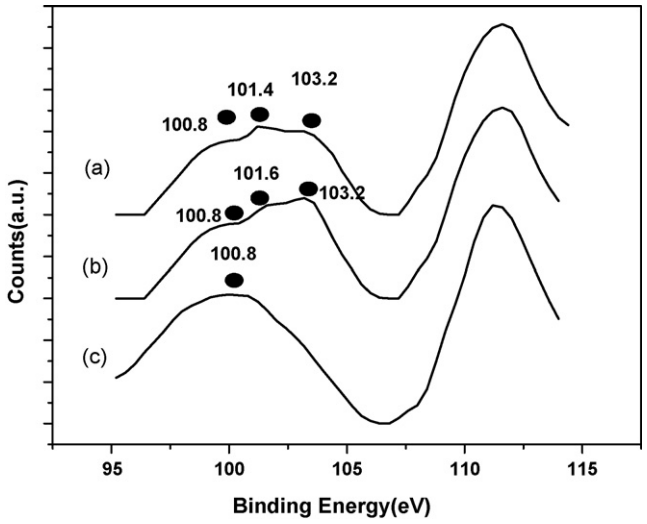

Fig. 8. Hg 4f7 XPS spectra of spent (a) AL-CBr ($\chi = 30\%$), (b) AL-CCl ($\chi = 30\%$), and (c) AL-C. (a) Hg 4f7 XPS spectra of the spent 30% NH_4Br doped $CuCoO_4$ loaded on γ-Al_2O_3. (b) Hg 4f7 XPS spectra of the spent 30% NH_4Cl doped $CuCoO_4$ loaded on γ-Al_2O_3. (c) Hg 4f7 XPS spectra of the spent $CuCoO_4$ loaded on γ-Al_2O_3.

HgO. Compared with AL-C, the mercury species adsorbed on spent AL-CCl or AL-CBr are more complex. The peaks near 101.4 eV can be attributed to $HgCl_2$ or $HgBr_2$, implying that anion Cl^- and Br^- have participated in Hg^0 oxidation reaction. Since blank samples AL-Cl and AL-Br do not show Hg^0 oxidation ability, anion Cl^- or Br^- must have been activated by N-doping AL-C.

Based on the above experiments, AL-CCl and AL-CBr's Hg^0 oxidation mechanism which is different from AL-C can be described as [14]:

$$Hg_{ad} + CuCo_2N_xO_{4-x} \rightarrow HgO_{ad} + CuCo_2N_xO_{3-x} \quad (7)$$

$$A_{ad} + \square\text{-}CuCo_2N_xO_{4-x} \rightarrow A\text{-}CuCo_2N_xO_{4-x} \quad (8)$$

$$Hg_{ad} + A\text{-}CuCo_2N_xO_{4-x} \rightarrow HgA_{ad} + CuCo_2N_xO_{4-x} \quad (9)$$

Wherein $\square$ is the active center of $CuCo_2N_xO_{4-x}$ such as oxygen vacancies, A_{ad} stands for Cl_{ad}^-, and Br_{ad}^-, A-$CuCo_2N_xO_{4-x}$ is the activated anion.

Step (7) is the reaction of adsorbed mercury with $CuCo_2N_xO_{4-x}$, forming adsorbed mercuric oxide and reducing the surface of sorbents. Step (8) is the activation of chemisorbed anion such as Cl_{ad}^- and Br_{ad}^- by $CuCo_2N_xO_{4-x}$. Step (9) is the reaction of adsorbed mercury with the activated anion. On the one hand, the nonmetal ions such as halide ions and nitrogen ions can replace some of the lattice O^{2-} ions. When Cl^- ion replaces an O^{2-} ion, the oxidation state of an adjacent cobalt or copper ion will drop from Co^{3+} to Co^{2+} or from Cu^{2+} to Cu^+ in order to maintain electroneutrality. The N-doping and halide-doping can cause Co or Cu oxidation state to change and hence affect the lattice oxygen activity. On the other hand, the nonmetal ions can occupy oxygen vacancies or dwell at interstitial sites. When a halide ion occupies an oxygen vacancy or an interstitial position, it will cause the oxidation state of an adjacent cobalt or copper ion to rise from Co^{2+} to Co^{3+} or from Cu^+ to Cu^{2+} [17,22].

Due to the electronegativity of Cl (3.16 V), the intercalation of Cl into the $CuCo_2O_4$ lattice will cause the valence electron density of O^{2-} to decrease. It shows that the presence of Cl in $CuCo_2O_4$ lattice matrix will weaken the cobalt–oxygen or copper–oxygen bonds. Since O^{2-} (radius, 1.40 Å) is less than Cl^- (radius, 1.81 Å), the doping of Cl^- into $CuCo_2O_4$ induce the expansion of a, b, and c dimensions. Both effects will result in an increase in the Co–O or Cu–O bond length. As a result, lattice O^{2-} become more active [22].

The N-doping and halide-doping can change the electric state of cobalt and copper. The increase of charge density on cobalt and copper atom causes their binding energy to decrease. The XPS data show that the Co 2p and Cu 2p binding energies of AL-CCl or AL-CBr are less than AL-C, which indicates that N-doping or halide-doping increases copper or cobalt atom charge density and lattice O^{2-} become more active. Meanwhile, Hg^0 can react with halide ions (i) dwelled at interstitial sites, (ii) located at lattice, (iii) activated by active centre of $CuCo_2N_xO_{4-x}$. This also increases the Hg^0 oxidation ability of sorbents [17,22].

4. Conclusions

NH_4Cl or NH_4Br doped AL-C turned out to show much higher Hg^0 oxidation abilities than AL-C, especially at low adsorption temperatures, and 30% is considered as the optimal NH_4Cl or NH_4Br adulteration value. The addition of 30% NH_4Cl or NH_4Br can improve the breakthrough time of AL-C from 26 h to 158 h or 208 h, respectively. AL-C, AL-CCl and AL-CBr all possess outstanding SO_2 anti-poisoning ability. The N-doping technology has not any adverse affect on either Co^{3+} or Cu^{2+}-octahedral cations structure of AL-C, which enables NH_4Cl or NH_4Br doped AL-C to inherit the SO_2 resistance ability of AL-C. The XRD and XPS analysis results indicate that N atoms have been doped into AL-C crystal lattice and anion Cl^- or Br^- can be activated by N-doped AL-C to oxidize elemental mercury.

Acknowledgment

We express our sincere thanks to the National Natural Science Foundation of China (No. 90510009) for its financial support.

References

[1] J.H. Pavlish, E.A. Sondreal, M.D. Mann, E.S. Olson, K.C. Galbreath, D.L. Laudal, S.A. Benson, Fuel Proc. Technol. 89–165 (2003) 82.
[2] D.V. Velzen, H. Langenkamp, G. Herb, Waste Manage. Res. 556–568 (2002) 20.
[3] Q. Wang, W. Shen, Z. Ma, Environ. Sci. Technol. 2711–2713 (2000) 34.
[4] S.E. Lindberg, W.J. Stratton, Environ. Sci. Technol. 49–57 (1998) 32.
[5] C.C. Travis, B.P. Blaylock, Toxicol. Environ. Chem. 203–215 (1995) 49.
[6] J.C.S. Chang, S.B. Ghorishi, Environ. Sci. Technol. 5763–5766 (2003) 37.
[7] P.S. Nolan, K.E. Redinger, G.T. Amrhein, G.A. Kudlac, Fuel Proc. Technol. 587–600 (2004) 85.
[8] R.D. Vidic, D.P. Siler, Carbon 3–14 (2001) 39.
[9] S.V. Krlshnan, B.K. Gullett, W. Jorewlczt, Environ. Sci. Technol. 1506–1512 (1994) 28.
[10] R.D. Vidic, J.B. McLaughlin, J. Air Waste Manage. Assoc. 241–250 (1996) 46.
[11] W.J. O'Dowd, R.A. Hargis, E.J. Granite, H.W. Pennline, Fuel Proc. Technol. 533–548 (2004) 85.
[12] E. Pitoniak, C.Y. Wu, D.W. Mazyck, K.W. Powers, W. Sigmund, Environ. Sci. Technol. 1269–1274 (2005) 39.
[13] J.W. Portzer, J.R. Albritton, C.C. Allen, R.P. Gupta, Fuel Proc. Technol. 621–630 (2004) 85.
[14] E.J. Granite, H.W. Pennline, R.A. Hargis, Ind. Eng. Chem. Res. 1020–1029 (2000) 39.
[15] Z. Shen, Z. Mei, J. Chen, T. Yuan, W. Wang, China Patent 200510024939.2 (CN1698931) (2005).
[16] S. Sato, R. Nakamura, S. Abe, Appl. Catal. A 131–137 (2005) 284.
[17] R. Asahi, T. Morikawa, T. Ohwaki, K. Aoki, Y. Taga, Science 269 (2001) 293.
[18] T. Ihara, M. Miyoshi, Y. Iriyama, O. Matsumoto, S. Sugihara, Appl. Catal. B 403 (2003) 42.
[19] C.D. Valentin, G. Pacchioni, A. Selloni, Phys. Rev. B 085116 (2004) 70.
[20] S.U.M. Khan, M. Al-Shahry, W.B.I. Jr., Science 2243–2245 (2002) 297.
[21] T. Umebayashi, T. Yamaki, H. Itoh, K. Asaia, Appl. Phys. Lett. 454–457 (2002) 81.
[22] H.X. Dai, C.F. Ng, C.T. Au, J. Catal. 251–266 (2001) 197.
[23] H.X. Dai, C.F. Ng, C.T. Au, J. Catal. 52–62 (2000) 189.
[24] D. Mehandjiev, B. Piperov, G. Bliznakov, Compt. Rend. Acad. Sci. Bulg. 1433 (1978) 31.
[25] S. Angelov, D. Mehandjiev, B. Piperov, V. Zarkov, A. Terlecki-Baričević, D. Jovanović, Ž. Jovanović, Appl. Catal. 431–437 (1985) 16.
[26] Z. Wang, W. Cai, X. Hong, X. Zhao, F. Xu, C. Cai, Appl. Catal. B 223–231 (2005) 57.
[27] S.B. Ghorishi, R.M. Keeney, S.D. Serre, B.K. Gullett, W.S. Jozewicz, Environ. Sci. Technol. 4454–4459 (2002) 36.
[28] F.E. Huggins, G.P. Huffman, G.E. Dunham, C.L. Senior, Energy Fuels 114–121 (1999) 13.
[29] H. Zeng, F. Jin, J. Guo, Fuel 143–146 (2004) 83.
[30] E. Zhecheva, S. Angelov, D. Mehandjiev, Thermochim. Acta 91–102 (1983) 67.